Intermolecular potential and second virial coefficient of the water-nitrogen complex

Akyl S. Tulegenov and Richard J. Wheatley[a)]
School of Chemistry, The University of Nottingham, Nottingham NG7 2RD, United Kingdom

Matthew P. Hodges
CCLRC Rutherford Appleton Laboratory, Chilton, Didcot, Oxfordshire OX11 0QX, United Kingdom

Allan H. Harvey
Physical and Chemical Properties Division, National Institute of Standards and Technology, Boulder, Colorado 80305

(Received 18 July 2006; accepted 8 January 2007; published online 6 March 2007)

The authors construct a rigid-body (five-dimensional) potential energy surface for the water-nitrogen complex using the systematic intermolecular potential extrapolation routine. The intermolecular potential is then extrapolated to the limit of a complete basis set. An analytic fit of this surface is obtained, and, using this, the global minimum energy is found. The minimum is located in an arrangement in which N_2 is near the H atom of H_2O, almost collinear with the OH bond. The best estimate of the binding energy is 441 cm^{-1} ($1\ cm^{-1} \approx 1.986\,43 \times 10^{-23}$ J). The extrapolated potential is then used to calculate the second cross virial coefficient over a wide temperature range (100–3000 K). These calculated second virial coefficients are generally consistent with experimental data, but for the most part the former have smaller uncertainties. © *2007 American Institute of Physics*. [DOI: 10.1063/1.2446843]

I. INTRODUCTION

The complex formed by water and molecular nitrogen has been a focus of several studies, both experimental and theoretical. Microwave spectroscopy of the $H_2O–N_2$ complex[1] suggested that there are four equivalent hydrogen-bonded structures, each having a nearly linear N–N–H–O geometry with a N–H distance of 2.42 Å and an OHN angle of 169°. In a combined experimental and theoretical examination of the infrared spectra of adsorbates on ice surfaces,[2] it was found that the bonding to water produces rather a small effect on the stretch vibration of N_2 by inducing a redshift of 5 cm^{-1} in the frequency. A semiempirical potential of the complex of water with N_2 was proposed by Sandler *et al.*[3] This work included *ab initio* calculations of the potential energy surface at the MP2 level of theory, analysis of different contributions to the interaction energy (exchange repulsion, electrostatic, dispersion, and induction), and the construction of a $H_2O–N_2$ potential function by fitting to *ab initio* data followed by adjustment against the experimental rotational and quadrupole coupling constants.[1] The potential was mapped for 110 different intermolecular configurations, as a function of the intermolecular distance. The final representation of the potential was given in terms of a model including 11 parameters. The minimum was located in an arrangement in which N_2 is adjacent to the H atom of H_2O, with a calculated well depth of 437 cm^{-1}.

In this work we present an *ab initio* intermolecular potential of the complex formed by $H_2O–N_2$, calculated at a higher level of theory than MP2. We then calculate the second virial coefficients using this potential and compare them to experimental results. This system is the first application of our systematic intermolecular potential extrapolation routine (SIMPER) to the treatment of complexes containing molecules with multiple bonds.

II. METHODS

A. Coordinate system

The coordinate system chosen for $H_2O\cdots N_2$ is shown in Fig. 1. The H_2O molecule lies in the xz plane, with the origin at the oxygen atom, and the hydrogen atoms having $z<0$. The N_2 center of mass location is defined by the spherical polar coordinates, R, θ, and ϕ, and the orientation of N_2 by the spherical polar angles, θ' and ϕ'. H_2O and N_2 are represented by rigid geometries averaged over the vibrational ground state. The H_2O geometry is recommended by Mas and Szalewicz:[4] $r_{OH}=1.8361a_0$ ($a_0 \approx 0.052\,917\,72$ nm) and the angle H–O–H=104.69°. The N_2 geometry is taken from Huber and Herzberg:[5] $r_{NN}=2.081a_0$.

B. *Ab initio* calculations

All calculations are performed using modified versions of the augmented correlation-consistent (aug-cc-pVXZ) basis sets of Dunning and co-workers,[6,7] which we call SP-aug-cc-pVXZ.[8] The SP basis sets are produced by modifying the Gaussian basis functions for each set of angular momentum functions above $p/d/d$ for the H/N/O atoms, by changing their exponents to be the same as the most diffuse exponents of the $p/d/d$ Gaussians of the same atom. This is done to produce faster convergence of the dispersion energy

a)Electronic mail: richard.wheatley@nottingham.ac.uk

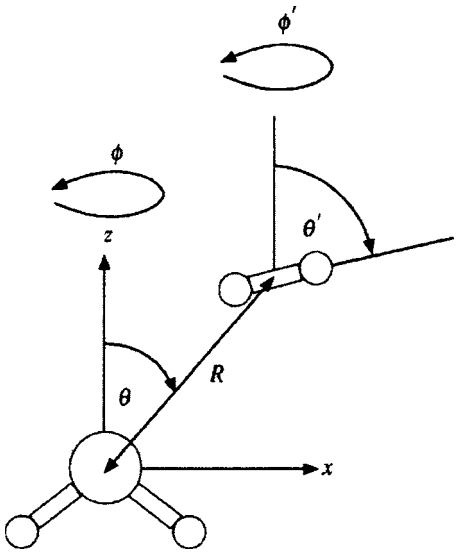

FIG. 1. Coordinate system used for H_2O-N_2.

to the limit of the complete basis set. The full counterpoise correction procedure of Boys and Bernardi[9] is used for the supermolecule calculations. The intermolecular potential is mapped for 12 288 different intermolecular configurations, as a function of the intermolecular distance and the set of intermolecular angular coordinates. The angular coordinates are sampled using 1024 entries in a four-dimensional Sobol sequence[10] over the range $[0,\pi]$ for θ, θ', ϕ', and $[0,\pi/2]$ for ϕ. The values of distance sampled are in the range $[5a_0,\ldots,9a_0]$, with step of $0.5a_0$, to sample the low repulsive wall and potential well region, and $[11a_0,\ldots,13a_0]$, with step of a_0, to ensure continuity with the long-range asymptotic behavior (see later).

The intermolecular potential is first evaluated at the MP2 supermolecule level of theory. The supermolecular MP2 calculations are carried out using the MOLPRO package.[11,12] The systematic extrapolation procedure is then applied to the MP2 intermolecular potential energy surface to obtain the SIMPER potential. This procedure is described next. For comparison, the intermolecular potential is also evaluated at the CCSD(T) supermolecule level of theory in the region of the global minimum.

C. The systematic intermolecular potential extrapolation routine

The starting point of the SIMPER method consists of splitting the total interaction energy estimated at a low level of theory in the supermolecule approach into components resembling counterparts from perturbation theory,

$$\Delta E_{\mathrm{tot}}^{\mathrm{low}} = \Delta E_{\mathrm{Coul}}^{\mathrm{low}} + \Delta E_{\mathrm{exch}}^{\mathrm{low}}. \tag{1}$$

Here $\Delta E_{\mathrm{tot}}^{\mathrm{low}}$ is the total interaction energy calculated using the "low-level" supermolecule method (MP2), with counterpoise correction, and $\Delta E_{\mathrm{Coul}}^{\mathrm{low}}$ is the MP2 "Coulomb" interaction energy.[13] As a result, the MP2 "exchange-repulsion" energy $\Delta E_{\mathrm{exch}}^{\mathrm{low}}$ is found indirectly from Eq. (1) at each point on the surface. There is no useful, unambiguous definition of the Coulomb and exchange-repulsion components of a supermolecule calculation, and several alternative methods for calculating the MP2 Coulomb and exchange-repulsion energies have been investigated[14] with the conclusion that the most reliable and efficient method for weak intermolecular forces is SIMPER-P2.

In the SIMPER-P2 method, the MP2 Coulomb interaction energy is calculated using Rayleigh-Schrödinger intermolecular perturbation theory to second order in the interaction. This use of perturbation theory is similar to methods such as symmetry-adapted perturbation theory (SAPT), but the SIMPER method is not closely related to SAPT. In particular, the SAPT method calculates the exchange-repulsion energy directly from perturbation theory, whereas the SIMPER method calculates it indirectly as the difference between the supermolecule energy and the Coulomb energy. Both methods have their own particular advantages, resulting from the different methods used to calculate the Coulomb and exchange-repulsion energies, but they have both been shown to be capable of producing high-quality potential energy surfaces for weak interactions.

Perturbation theory is then used to divide the calculated MP2 Coulomb energy rigorously into first-order electrostatic and second-order induction and dispersion energy contributions,[15]

$$\Delta E_{\mathrm{Coul}}^{\mathrm{low}} = \Delta E_{\mathrm{elst}}^{\mathrm{low}} + \Delta E_{\mathrm{ind}}^{\mathrm{low}} + \Delta E_{\mathrm{disp}}^{\mathrm{low}}, \tag{2}$$

The aim of the SIMPER method is to improve the Coulomb and exchange-repulsion components of the total interaction energy, leading to approximate high-level terms which can then be added to give the final intermolecular potential

$$\Delta E_{\mathrm{tot}}^{\mathrm{high}} = \Delta E_{\mathrm{elst}}^{\mathrm{high}} + \Delta E_{\mathrm{ind}}^{\mathrm{high}} + \Delta E_{\mathrm{disp}}^{\mathrm{high}} + \Delta E_{\mathrm{exch}}^{\mathrm{high}}. \tag{3}$$

The methods used in SIMPER-P2 to calculate each term in Eq. (3) are described next; they differ slightly from the procedure outlined in Ref. 14, as the description of the induction energy has been improved.

1. The electrostatic energy

The first-order low-level Coulomb interaction energy is obtained by expanding the supermolecule MP2 energy to first order in the interaction. It can be expressed in terms of densities,

$$\begin{aligned}\Delta E_{\mathrm{elst}}^{\mathrm{low}} = &\int \rho_A^{\mathrm{SCF+MP2}}(\mathbf{r}) v_B(\mathbf{r}) d\mathbf{r} + \int \rho_B^{\mathrm{SCF+MP2}}(\mathbf{r}) v_A(\mathbf{r}) d\mathbf{r} \\ &+ \int\int \rho_A^{\mathrm{SCF}}(\mathbf{r}_1) \frac{1}{r_{12}} \rho_B^{\mathrm{SCF}}(\mathbf{r}_2) d\mathbf{r}_1 d\mathbf{r}_2 \\ &+ \int\int \rho_A^{\mathrm{MP2}}(\mathbf{r}_1) \frac{1}{r_{12}} \rho_B^{\mathrm{SCF}}(\mathbf{r}_2) d\mathbf{r}_1 d\mathbf{r}_2 \\ &+ \int\int \rho_A^{\mathrm{SCF}}(\mathbf{r}_1) \frac{1}{r_{12}} \rho_B^{\mathrm{MP2}}(\mathbf{r}_2) d\mathbf{r}_1 d\mathbf{r}_2 + V_{\mathrm{nuc}},\end{aligned} \tag{4}$$

where V_{nuc} is the intermolecular nuclear repulsion, v_X is the nuclear potential of molecule X, ρ_X^{SCF} is the self-consistent-field (SCF) electron density of molecule X, and ρ_X^{MP2} is the MP2 correction to the density of molecule X obtained from relaxed orbitals.[16] This low-level electrostatic energy is re-

placed in the total intermolecular potential by using more accurate monomer densities,

$$\Delta E_{\mathrm{elst}}^{\mathrm{high}} = \int \rho_A^{\mathrm{SCF+CCSD}}(\mathbf{r}) v_B(\mathbf{r}) d\mathbf{r} + \int \rho_B^{\mathrm{SCF+CCSD}}(\mathbf{r}) v_A(\mathbf{r}) d\mathbf{r} + \int\int \rho_A^{\mathrm{SCF+CCSD}}(\mathbf{r}_1) \frac{1}{r_{12}} \rho_B^{\mathrm{SCF+CCSD}}(\mathbf{r}_2) d\mathbf{r}_1 d\mathbf{r}_2 + V_{\mathrm{nuc}}, \tag{5}$$

where $\rho_X^{\mathrm{SCF+CCSD}}$ is the total CCSD electron density of molecule X.

2. The exchange-repulsion energy

Exchange repulsion is the dominant repulsive component of the intermolecular potential and the most difficult one to calculate explicitly. Within SIMPER we apply the overlap model to relate the low-level exchange-repulsion energy to the electron density overlap in the form

$$\Delta E_{\mathrm{exch}}^{\mathrm{low}}(R,\Omega) = K^{\mathrm{low}}(R,\Omega) \times S_\rho^{\mathrm{low}}(R,\Omega), \tag{6}$$

where $S_\rho^{\mathrm{low}}(R,\Omega)$ is the electron density overlap and $K^{\mathrm{low}}(R,\Omega)$ is a function of the intermolecular coordinates which is found from Eq. (6) at each point on the surface. The high-level and low-level overlap parameters are assumed to be equal at each point,

$$K^{\mathrm{high}}(R,\Omega) = K^{\mathrm{low}}(R,\Omega). \tag{7}$$

The high-level exchange-repulsion energy is then calculated as

$$\Delta E_{\mathrm{exch}}^{\mathrm{high}}(R,\Omega) = K^{\mathrm{low}}(R,\Omega) \times S_\rho^{\mathrm{high}}(R,\Omega), \tag{8}$$

where the effects of anisotropy are fully taken into account and no fitting is used. It may be noted that $S_\rho^{\mathrm{low}}(R,\Omega)$ depends entirely on monomer charge densities and is relatively inexpensive to calculate. As the low level is the supermolecule MP2 method, $S_\rho^{\mathrm{low}}(R,\Omega)$ consists of the overlap between SCF electron densities, plus the overlap between the SCF electron density on one molecule and the MP2 electron density correction on the other, and vice versa. $S_\rho^{\mathrm{high}}(R,\Omega)$ is defined in a similar manner to the high-level electrostatic energy and corresponds to the overlap of the total CCSD electron densities on both molecules.

We note that the "exchange-repulsion energy" defined by SIMPER-P2 contains some Coulomb contributions, namely, the induction energy at third and higher orders. It would not be helpful to treat high orders of Coulomb and exchange energies separately, since the total Coulomb energy to infinite order is unphysically large and negative,[17] so the exchange energy is unphysically large and positive, and the two almost cancel each other. Instead, the (somewhat arbitrary) decision to combine all terms above second order is implemented in SIMPER-P2. We have investigated using separate third-order Coulomb energy contributions, leading to a method called SIMPER-P3, but the results are not much different from SIMPER-P2, and neither method gives consistently better results, so the computationally cheaper SIMPER-P2 method is preferred.

3. The induction energy

At low level, the induction energy is an identifiable part of the second-order MP2 Coulomb interaction energy (the remainder is the dispersion energy, discussed below). It is a result of polarization of the molecule $A(B)$ in the field produced by the charge density of $B(A)$. The low-level induction energy is the sum of the SCF and MP2 induction energies

$$\Delta E_{\mathrm{ind}}^{\mathrm{low}} = \Delta E_{\mathrm{ind}}^{\mathrm{SCF}} + \Delta E_{\mathrm{ind}}^{\mathrm{MP2}}. \tag{9}$$

The SCF induction energy can be expressed in terms of static response functions and the potential due to the zero-order charge densities

$$\Delta E_{\mathrm{ind}}^{\mathrm{SCF}} = -\tfrac{1}{2}\sum_{ijab} \Pi_{ia,jb}^{(A),\mathrm{CHF}} V_{i,a}^{(B),\mathrm{SCF}} V_{j,b}^{(B),\mathrm{SCF}} - \tfrac{1}{2}\sum_{ijab} \Pi_{ia,jb}^{(B),\mathrm{CHF}} V_{i,a}^{(A),\mathrm{SCF}} V_{j,b}^{(A),\mathrm{SCF}}, \tag{10}$$

where $\Pi^{(X),\mathrm{CHF}}$ is the coupled Hartree-Fock (CHF) response function[18] of molecule X, i and j are occupied orbitals, a and b are virtual orbitals, and $V^{(X),\mathrm{SCF}}$ is the potential produced by the SCF density of molecule X. The first term in Eq. (10) corresponds to the polarization of molecule A and the second term to the polarization of molecule B. The MP2 induction energy can be represented similarly as a sum of four components

$$\Delta E_{\mathrm{ind}}^{\mathrm{MP2}} = -\sum_{ijab} \Pi_{ia,jb}^{(A),\mathrm{CHF}} V_{i,a}^{(B),\mathrm{MP2}} V_{j,b}^{(B),\mathrm{SCF}} - \tfrac{1}{2}\sum_{pqrs} \Pi_{pq,rs}^{(A),\mathrm{MP2}} V_{p,q}^{(B),\mathrm{SCF}} V_{r,s}^{(B),\mathrm{SCF}} - \sum_{ijab} \Pi_{ia,jb}^{(B),\mathrm{CHF}} V_{i,a}^{(A),\mathrm{MP2}} V_{j,b}^{(A),\mathrm{SCF}} - \tfrac{1}{2}\sum_{pqrs} \Pi_{pq,rs}^{(B),\mathrm{MP2}} V_{p,q}^{(A),\mathrm{SCF}} V_{r,s}^{(A),\mathrm{SCF}}, \tag{11}$$

where $\Pi^{(X),\mathrm{MP2}}$ is the MP2 response function of molecule X, p, q, r, and s are occupied or virtual orbitals, and $V^{(X),\mathrm{MP2}}$ is the operator of the potential produced by the MP2 density of molecule X (note that terms involving MP2 response to MP2 density are not present).

The induction energy is recalculated in the SIMPER procedure by using accurate densities, but retaining the MP2 response functions,

$$\Delta E_{\mathrm{ind}}^{\mathrm{high}} = -\tfrac{1}{2}\sum_{ijab} \Pi_{ia,jb}^{(A),\mathrm{CHF}} V_{i,a}^{(B),\mathrm{SCF+CCSD}} V_{j,b}^{(B),\mathrm{SCF+CCSD}} - \tfrac{1}{2}\sum_{pqrs} \Pi_{pq,rs}^{(A),\mathrm{MP2}} V_{p,q}^{(B),\mathrm{SCF+CCSD}} V_{r,s}^{(B),\mathrm{SCF+CCSD}} - \tfrac{1}{2}\sum_{ijab} \Pi_{ia,jb}^{(B),\mathrm{CHF}} V_{i,a}^{(A),\mathrm{SCF+CCSD}} V_{j,b}^{(A),\mathrm{SCF+CCSD}} - \tfrac{1}{2}\sum_{pqrs} \Pi_{pq,rs}^{(B),\mathrm{MP2}} V_{p,q}^{(A),\mathrm{SCF+CCSD}} V_{r,s}^{(A),\mathrm{SCF+CCSD}}, \tag{12}$$

where $V^{(X),\mathrm{SCF+CCSD}}$ is the operator of the potential produced by the total CCSD density of molecule X.

4. The dispersion energy

The dispersion energy arises from intermolecular electron correlation. At low level, it is part of the second-order MP2 Coulomb interaction energy and can be expressed as

$$\Delta E_{\mathrm{disp}}^{\mathrm{low}} = -\sum_{i,a\in A}\sum_{j,b\in B}\frac{\langle\psi_{\mathrm{SCF}}^{(0)}|V|\psi_{ij}^{ab}\rangle\langle\psi_{ij}^{ab}|V|\psi_{\mathrm{SCF}}^{(0)}\rangle}{\epsilon_a+\epsilon_b-\epsilon_i-\epsilon_j}, \tag{13}$$

where $|\psi_{ij}^{ab}\rangle$ in second-quantized form is $a^{+}ib^{+}j|\psi_{\mathrm{SCF}}^{(0)}\rangle$, V is the intermolecular Coulomb electron repulsion operator, ϵ is the energy of occupied (i,j) and virtual (a,b) orbitals, and $\psi_{\mathrm{SCF}}^{(0)}$ is the zero-order dimer SCF wave function.

In order to estimate the dispersion energy at a higher level of theory, we use a damped multipolar representation

$$\Delta E_{\mathrm{disp}}^{\mathrm{low}}(R,\Omega) = -\sum_{n} C_n^{\mathrm{low}}(\Omega) f_n^{\mathrm{low}}(\Omega,R) R^{-n}, \tag{14}$$

where C_n^{low} correspond to the supermolecule MP2 dispersion energy coefficients and $f_n^{\mathrm{low}}(R)$ are the damping functions expressed in the form of incomplete Gamma functions

$$f_n^{\mathrm{low}}(\Omega,R) = 1 - e^{-b^{\mathrm{low}}(\Omega,R)R}\sum_{k=0}^{n}\frac{(b^{\mathrm{low}}(\Omega,R)R)^k}{k!}. \tag{15}$$

The dispersion energy coefficients C_n^{low} are calculated as a sum over states using uncoupled Hartree-Fock transition multipoles and transition energies. The nonexpanded low-level dispersion energy $\Delta E_{\mathrm{disp}}^{\mathrm{low}}$ is calculated at each point on the potential energy surface from Eq. (13). As a result, the parameter b^{low} in the damping functions is the only unknown quantity in Eq. (14), so it is found exactly from the condition that the sum of the series on the right-hand side must equal the calculated energy on the left. In this work, n takes all values from 6 up to 16. It must be noted that Eq. (14) is nonlinear for b, so in principle multiple solutions are possible, but in practice only one solution is found in the physically reasonable range from 1 to 2 a.u. for each of the 12 288 calculations.

The high-level dispersion interaction energy is then represented in a form analogous to Eq. (14), but including high-level damping functions and dispersion energy coefficients. As a result, the extrapolation process consists of calculating high-level dispersion energy coefficients C_n^{high} and extrapolation of the low-level damping parameters b^{low} to high level.

In order to obtain b^{high} we apply the length scaling approximation[14]

$$b^{\mathrm{high}}\left(\frac{C_8^{\mathrm{high}}}{C_6^{\mathrm{high}}}\right)^{1/2} = b^{\mathrm{low}}\left(\frac{C_8^{\mathrm{low}}}{C_6^{\mathrm{low}}}\right)^{1/2}. \tag{16}$$

This involves no extra computational effort, as the low-level dispersion energy coefficients and damping parameters are known, and the high-level dispersion energy coefficients are used in the expression for the high-level dispersion energy anyway.

The time-dependent CISD (TD-CISD) method is used in SIMPER for calculating high-level dispersion energy coefficients, since previous studies have shown it to give accurate results.[14] The details of the procedure for calculating the TD-CISD dispersion energy coefficients are described in Ref. 19.

The high-level damped dispersion energy is calculated from high-level damping parameters and high-level dispersion energy coefficients

$$\Delta E_{\mathrm{disp}}^{\mathrm{high}} = -\sum_{n} C_n^{\mathrm{high}} f_n^{\mathrm{high}}(R) R^{-n}, \tag{17}$$

where C_n^{high} are the high-level CISD dispersion energy coefficients and

$$f_n^{\mathrm{high}}(R) = 1 - e^{-b^{\mathrm{high}}R}\sum_{k=0}^{n}\frac{(b^{\mathrm{high}}R)^k}{k!}. \tag{18}$$

This step completes the extrapolation procedure, and the SIMPER potential is then given by Eq. (3).

D. Fitting the potential energy surface

The intermolecular potential energy surface is fitted to an expansion in atom-centered form, with centers on the hydrogen atoms and oxygen atom of the water molecule and both nitrogen atoms,

$$\Delta E_{\mathrm{acr}}(R,\theta,\phi,\theta',\phi') = \sum_{a=\mathrm{H}^1,\mathrm{H}^2,\mathrm{O}}\sum_{b=\mathrm{N}^1,\mathrm{N}^2}\sum_{i}\sum_{\Lambda} C_{ab,i}^{\Lambda} S_{ab}^{\Lambda}(\Omega_{ab}) R_{ab}^{-i}, \tag{19}$$

where S is an orientation function[20] which introduces anisotropy into the atom-atom interactions. Local axes on the atoms of water are defined to be parallel to the fixed axes defined in Fig. 1, but the local x and y axes of the left-hand hydrogen atom are reversed. A local z axis is defined for each nitrogen atom, which points away from the center of the nitrogen molecule. There are 94 distinct S functions, with angular momenta $l \leqslant 2$ for H–N and $l \leqslant 3$ for O–N. The distance dependence is described by six R_{ab}^{-i} functions, with $i = 2, 3, 4, 6, 8, 12$. The fit to all 12 288 energies therefore uses 564 independent parameters, and minimizes the Boltzmann weighted error,

$$\Omega^2 = \frac{\Sigma_g w_g (E_{\mathrm{fit}}(g) - E_{\mathrm{calc}}(g))^2}{\Sigma_g w_g}, \tag{20}$$

with weights given by

$$w_g = e^{-E_{\mathrm{calc}}(g)/E_b}, \tag{21}$$

where $E_b = 658\ \mathrm{cm}^{-1}$. This is chosen to ensure a close fit to the potential well and to the part of the repulsive wall that is sampled in the virial coefficient calculations. The best fit gives $\Omega \approx 0.56\ \mathrm{cm}^{-1}$. Although the atom-centered representation provides an accurate description of the potential at short and intermediate ranges, it fails to describe the asymptotic potential at long range. In order to ensure a proper asymptotic behavior of the potential we use the switching function[21]

$$F(R) = \{1 + \tanh[6(R/a_0) - 78]\}/2 \tag{22}$$

to move to a molecule-centered representation of the potential at long range, where we switch to the multipolar approximation

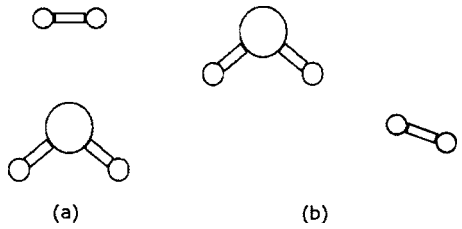

FIG. 2. Geometry of the H_2O-N_2 complex in (a) O and (b) H geometries.

$$\Delta E_{\text{mult}}(R,\Omega) = \sum_{n=4}^{8} \frac{C_n(\Omega)}{R^n}, \tag{23}$$

where $C_n(\Omega)$ coefficients comprise the "high-level" multipolar electrostatic, induction, and dispersion terms, and $\Omega = \{\theta, \phi, \theta', \phi'\}$. Thus, the final form of the intermolecular potential is

$$\Delta E(R,\Omega) = F(R)\Delta E_{\text{mult}}(R,\Omega) + (1 - F(R))\Delta E_{\text{acr}}(R,\Omega), \tag{24}$$

where $\Delta E_{\text{acr}}(R,\Omega)$ is the representation of the potential in the atom-centered form and $\Delta E_{\text{mult}}(R,\Omega)$ is the multipolar interaction energy. This representation of the potential ensures a proper description of the long-range interaction energy, which is important for the description of the second virial coefficients. The parameters for the fitted potential energy function and a FORTRAN subroutine to evaluate it are available as supplementary material via EPAPS.[22]

III. RESULTS

A. The potential energy surface

A qualitative understanding of the low-energy areas of the intermolecular potential energy surface can be obtained by considering the electrostatic interaction between charge distributions of N_2 and H_2O.[2] The quadrupole moment of the N_2 molecule can be represented by a set of two negative charges on the N atoms and a positive charge in the middle of the N–N bond. By placing a negative charge on O and two positive charges on the H atoms of H_2O it is possible to rationalize that the minimum energy configuration should involve a hydrogen-bonded structure in which a positive charge on a H atom contacts a negatively charged N atom. This is called the H geometry and is shown in Fig. 2. In an alternative arrangement the negatively charged O atom can point to the middle of the N–N bond. If the monomers are coplanar, the interaction is reinforced by the attraction between the negative charges on the N atoms and positive charges on the H atoms. Such an arrangement occurs in the O geometry (see Fig. 2).

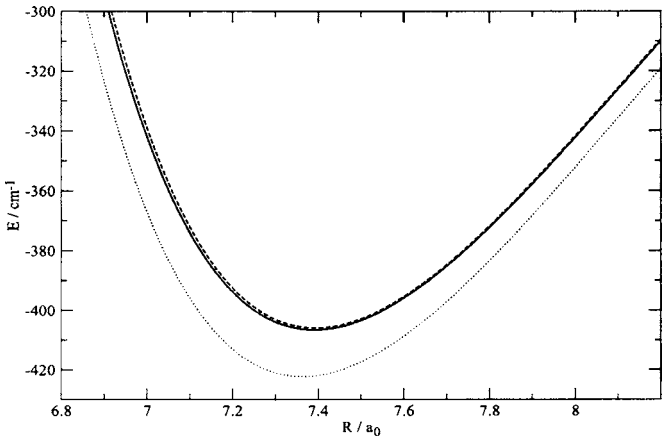

FIG. 4. Radial dependence of the potential in the vicinity of the H geometry (θ=120, θ'=120, ϕ=0, ϕ'=0) calculated using the SP-AVQZ basis set. Solid line: CCSD(T); dashed line: SIMPER; dotted line: MP2.

In the MP2 and SIMPER potential energy surfaces, the global minimum occurs in the vicinity of the H geometry, in which N_2 is located almost collinearly at the hydrogen end of the OH bond. The angular dependence of the distance-optimized potential calculated at three levels of theory in the vicinity of the H configuration is shown in Fig. 3, and the radial dependence is shown in Fig. 4. The O geometry is found to be a saddle point. The angular dependence of the distance-optimized potential calculated at three levels of theory in the vicinity of the O configuration is shown in Fig. 5, and the radial dependence is shown in Fig. 6. The H and O geometries are also shown in Fig. 7, where the potential is presented as a function of θ and θ' angles, optimized with

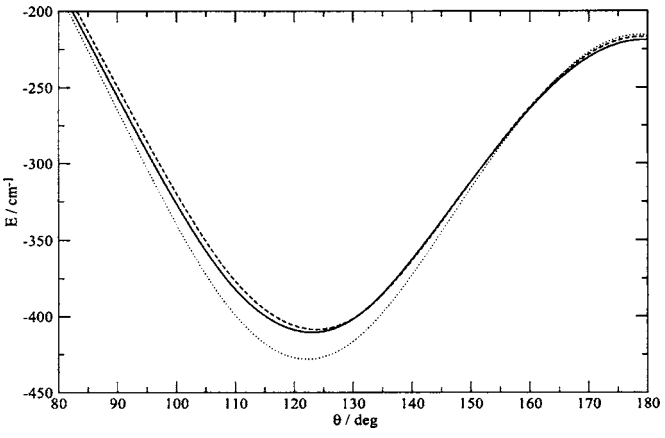

FIG. 3. Angular dependence of the distance-optimized potential in the vicinity of the H geometry ($\theta=\theta'$, ϕ=0, ϕ'=0), calculated using the SP-AVQZ basis set. Solid line; CCSD(T); dashed line: SIMPER; dotted line: MP2.

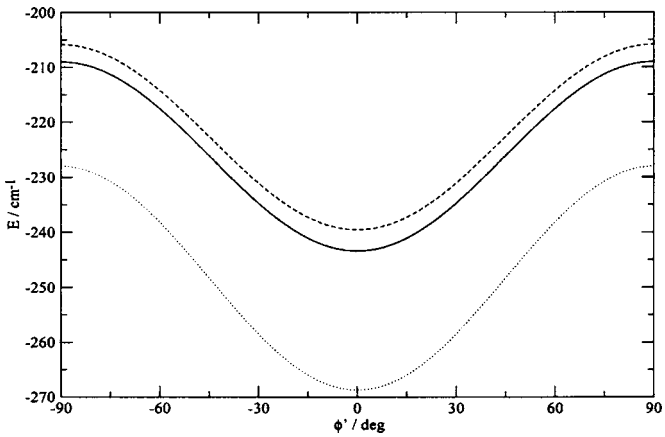

FIG. 5. Angular dependence of the potential in the vicinity of the O geometry (θ=0, θ'=90, ϕ=0), calculated using the SP-AVQZ basis set. Solid line: CCSD(T); dashed line: SIMPER; dotted line: MP2.

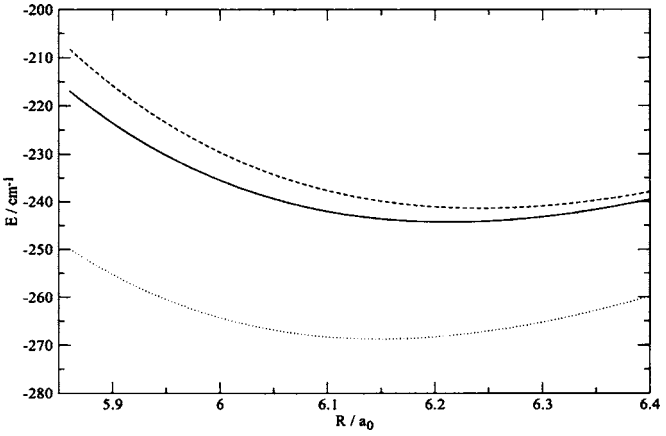

FIG. 6. Radial dependence of the potential in the vicinity of the O configuration (θ=0, θ'=90, ϕ=0, ϕ'=0), calculated using the SP-AVQZ basis set. Solid line: CCSD(T); dashed line: SIMPER; dotted line: MP2.

respect to other coordinates (R, ϕ, ϕ'). The O geometry corresponds to θ=0° and θ'=90°. Note that Fig. 3 shows the potential near the global minimum, not exactly at the minimum. The global minimum in the H configuration corresponds to θ=116.2° and θ'=106.0° with a well depth (from the fit) of 433 cm^{-1}.

We note that the depth of the MP2 potential in the H and O configurations is overestimated compared to the CCSD(T) values. Application of SIMPER to the low-level MP2 interaction energies gives results that are in excellent agreement with the CCSD(T) potential, but at much lower computational cost: the most time-consuming part of the SIMPER method is the calculation of the MP2 supermolecule energies, followed by the MP2 induction energies, both of which scale as the fifth power of system size.

In order to investigate the difference between the MP2 and CCSD(T) energies, it is useful to examine the four components of the total potential at MP2 and SIMPER levels of theory. Tables I and II show that at both orientations the electrostatic energy is a major attractive component. Qualitatively, the difference may be attributed to the fact that the MP2 density is more spatially extended than the CCSD density, which results in larger multipole moments. This also produces a larger electron density overlap, which increases the MP2 exchange-repulsion energy.

In order to estimate the intermolecular potential in the complete basis set limit we apply the two-point extrapolation formula of Bak *et al.*[23] to the intermolecular potentials obtained from SP-AVTZ and SP-AVQZ basis sets,

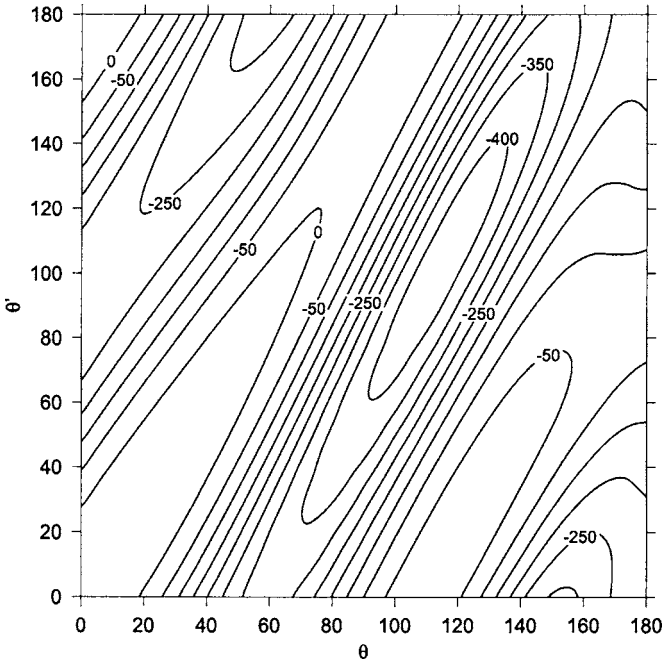

FIG. 7. The contour plot of the SIMPER potential energy surface calculated using the SP-AVQZ basis set for the case when both molecules are located in the *xz* plane. The values at each angular point are distance optimized and the potential is in units of cm^{-1}.

$$\Delta E_{x-1,x} = \frac{x^3 \Delta E_x - (x-1)^3 \Delta E_{x-1}}{x^3 - (x-1)^3}, \tag{25}$$

where x is the cardinality of the basis set (x=3 for SP-AVTZ and x=4 for SP-AVQZ). Results from this extrapolation are shown in Table III. The effect of basis set extrapolation is to shift the potential energy toward more negative values, although the difference between the SP-AVQZ basis set and the estimated complete basis set limit is small compared to the difference between the MP2 and CCSD(T) methods. The SIMPER method appears to behave stably with respect to enlargement of the basis set. Extrapolating from the SP-AVQZ basis set to the complete basis set limit increases the well depth by no more than 2%.

The extrapolated potential energy surface is fitted using the scheme described in Sec. II D, giving $\Omega \approx 0.56$ cm^{-1}. The SIMPER well depth from the fit is 441 cm^{-1}. This entirely *ab initio* value agrees closely with the well depth of 437 cm^{-1} for the potential of Sandler *et al.*,[3] which was fitted to experimental data. We use this fit to the extrapolated potential energy surface to calculate second virial coefficients for the H_2O-N_2 interaction.

TABLE I. Components of the intermolecular potential (cm^{-1}) in the vicinity of the H geometry for the H_2O-N_2 complex, obtained with the SP-AVQZ basis set. The angle θ is given in degrees and the total potential is distance optimized.

$\theta=\theta'$	ΔE_{elst}^{low}	ΔE_{elst}^{high}	ΔE_{ind}^{low}	ΔE_{ind}^{high}	ΔE_{disp}^{low}	ΔE_{disp}^{high}	ΔE_{exch}^{low}	ΔE_{exch}^{high}
90.0	−238.3	−222.0	−77.4	−76.7	−270.9	−254.2	321.9	302.7
120.0	−550.7	−517.8	−190.2	−190.8	−374.4	−351.9	688.3	650.8
150.0	−383.0	−356.6	−112.5	−114.8	−294.5	−281.9	474.0	437.8
180.0	−209.9	−193.1	−48.5	−50.6	−210.2	−203.0	252.7	227.3

TABLE II. Components of the intermolecular potential (cm^{-1}) in the vicinity of the O geometry, obtained with the SP-AVQZ basis set. The angle ϕ is given in degrees and $R=5.858\,151a_0$.

ϕ	ΔE_{elst}^{low}	ΔE_{elst}^{high}	ΔE_{ind}^{low}	ΔE_{ind}^{high}	ΔE_{disp}^{low}	ΔE_{disp}^{high}	ΔE_{exch}^{low}	ΔE_{exch}^{high}
0	−367.9	−335.7	−98.9	−99.1	−411.8	−374.4	629.1	601.3
30	−355.5	−324.9	−99.9	−99.9	−411.6	−374.5	628.9	600.9
60	−330.8	−303.4	−101.5	−101.6	−411.1	−374.7	628.5	600.1
90	−318.6	−292.8	−102.3	−102.3	−410.9	−374.7	628.2	599.7

B. Second virial coefficients

1. Experiment

Information about B_{12} for this system can be obtained from measurements of the solubility of ice[24–28] or liquid water[24,27–32] in gaseous nitrogen. The procedures for deriving B_{12} from these data and estimating its uncertainty have been described previously,[33,34] and the results are given in Table IV. The solubility of nitrogen in liquid water is calculated from Henry's constants measured by Rettich *et al.*[35] below 50 °C and from Fernández-Prini *et al.*[36] at higher temperatures. For the data of Gillespie and Wilson,[30] the measured coexisting liquid compositions are used. The uncertainties in Table IV (standard uncertainty with coverage factor of 2) reflect only the measurement of water content in the gas phase; additional factors such as neglect of higher virial coefficients are not included.

The data of Rigby and Prausnitz[29] were reduced to B_{12} by the authors and we adopt their values (including uncertainties), which are also shown in Table IV. Rigby and Prausnitz did not explain how they defined their reported uncertainties; it is possible that they correspond to one standard deviation, in which case the uncertainties for those points in Table IV should be doubled to be on the same footing as the other data. We assume that the 2002 data of Blanco *et al.*[28] supersede the 1999 data of Blanco *et al.*,[37] which scatter badly. For data that did not fall exactly on isotherms,[28,32] the temperature dependence of the vapor pressure of water[38] is used to adjust the reported vapor mole fraction at individual points to the nominal temperature adopted for the isotherm.

Plyasunov and Shock[39] derived B_{12} from many of these data sources, using somewhat different data reduction procedures. Their values of B_{12} often differ from those in Table IV, but the differences are always within their mutual uncertainties (barely so for a few of the points). The lack of a standard best procedure for deriving B_{12} from solubility data is another reason to prefer *ab initio* values if they can be calculated reliably.

At high temperatures, values of B_{12} may also be deduced from volumetric measurements on mixtures as a function of pressure. Table IV also includes three values that were derived by Abdulagatov *et al.*[40] in this manner. Uncertainties in B_{12} were not reported, so this information is left blank in Table IV.

Information about B_{12} can also come from vapor-phase enthalpy-of-mixing data, which can yield the quantity

$$\phi_{12} = B_{12} - T\frac{dB_{12}}{dT} \tag{26}$$

when extrapolated to low pressure. At temperatures from approximately 373 to 423 K, values of ϕ_{12} were reported by Richards *et al.*[41] and later reanalyzed by Wormald and Lancaster.[42] In Table V, we give the values from their re-

TABLE III. Interaction energies for H_2O-N_2 (cm^{-1}), calculated at different levels of theory, as described in the text, including extrapolation to the complete basis set limit. The selected geometries are planar, with $\phi=\phi'=0$.

		MP2			SIMPER			CCSD(T)		
R/a_0	$\theta=\theta'$	TZ	QZ	CBS	TZ	QZ	CBS	TZ	QZ	CBS
12.0	0	20.4	20.5	20.7	18.8	18.8	18.8	18.7	18.7	18.6
12.0	30	15.8	15.8	15.9	14.6	14.5	14.5	14.3	14.3	14.3
7.5	60	−52.6	−55.5	−57.6	−54.2	−57.4	−59.7	−56.4	−58.8	−60.6
7.3	90	−258.2	−264.7	−269.4	−246.6	−250.8	−253.9	−249.9	−255.9	−260.2
7.3	110	−391.5	−399.1	−404.7	−376.6	−379.6	−381.8	−374.8	−382.0	−387.2
7.3	120	−418.6	−427.1	−433.3	−405.6	−409.2	−411.9	−400.6	−408.7	−414.6
7.4	130	−408.3	−416.3	−422.2	−399.6	−404.1	−407.5	−393.7	−401.6	−407.3
7.5	150	−308.6	−316.1	−321.6	−306.7	−313.3	−318.2	−304.3	−311.8	−317.3
7.7	180	−210.8	−215.9	−219.6	−211.6	−217.2	−221.3	−214.0	−219.1	−222.9
7.0	128	−352.6	−367.0	−377.5	−337.5	−344.4	−349.4	−327.6	−341.9	−352.4
8.0	128	−349.0	−352.2	−354.4	−341.0	−342.8	−344.2	−339.4	−342.2	−344.3
9.0	128	−202.4	−202.3	−202.3	−195.3	−195.1	−194.9	−195.5	−195.4	−195.2
10.0	128	−113.5	−113.2	−112.9	−108.1	−107.8	−107.5	−108.6	−108.1	−107.7
11.0	128	−66.9	−66.6	−66.3	−63.1	−62.7	−62.4	−63.4	−63.0	−62.8
12.0	128	−41.7	−41.5	−41.3	−39.0	−38.8	−38.6	−39.3	−39.1	−38.9
13.0	128	−27.4	−27.2	−27.1	−25.4	−25.3	−25.2	−25.7	−25.6	−25.5

TABLE IV. $H_2O\cdots N_2$ second virial coefficients B_{12} and their uncertainties ΔB_{12} derived from experimental data. Temperatures are given in K, and B_{12} and their uncertainties ΔB_{12} in $cm^3\ mol^{-1}$.

T	B_{12}	ΔB_{12}	Reference	T	B_{12}	ΔB_{12}	Reference
223.16	−77.4	19.0	26	288.56	−37.0	5.2	31
233.16	−62.3	17.5	26	293.10	−28.7	8.1	32
233.16	−151.5	58.6	25	293.15	−29.2	2.6	27
243.16	−51.6	10.9	26	293.16	−70.7	10.0	24
243.16	−121.4	23.9	24	293.38	−32.9	3.0	31
248.15	−50.6	38.0	27	298.10	−31.2	2.3	31
253.15	−57.7	10.8	26	298.14	−40.0	6.0	29
253.15	−80.7	13.6	25	304.36	−21.3	9.3	32
253.15	−43.5	25.1	27	310.92	−32.4	5.3	30
258.15	−38.5	23.0	27	311.06	−26.1	3.0	31
263.1	−15.4	28.6	28	313.26	−23.2	9.1	32
263.15	−40.9	12.7	26	322.93	−26.9	8.9	32
263.15	−69.5	14.0	25	323.09	−20.1	3.8	31
263.15	−49.7	10.4	27	323.13	−28.0	5.0	29
268.15	−45.3	9.1	27	332.52	−19.3	10.6	32
268.5	38.4	28.6	28	342.31	−7.5	9.7	32
271.15	−49.7	11.4	26	348.12	−20.0	4.0	29
273.0	−18.7	28.8	28	351.95	−32.6	10.2	32
273.15	−51.9	14.5	25	363.00	−19.7	12.5	32
273.15	−32.3	6.0	27	366.46	−15.0	6.2	30
278.15	−29.9	5.1	27	373.12	−15.5	3.0	29
278.3	−7.1	30.3	28	422.00	−4.9	8.9	30
282.43	−35.5	2.0	31	477.55	−8.6	16.0	30
282.99	−33.1	8.3	32	523.15	3.0		40
283.15	−31.2	3.6	27	573.15	3.3		40
283.16	−65.8	9.2	24	663.15	6.5		40
283.3	24.1	40.7	28				

analysis, along with their reported uncertainties.

At higher temperatures and pressures, excess enthalpies for water-nitrogen mixtures were reported by Lancaster and Wormald,[43] who reanalyzed earlier measurements[44] and supplemented them with new data. Similar measurements extending above 900 K were reported by Wilson and Brady.[45] As described previously,[34] we extrapolate these data to zero pressure in order to extract ϕ_{12}. Those values are also given in Table V; their uncertainties result primarily from uncertainty in the zero-pressure extrapolation.

For all the calculations of this section, $B(T)$ and dB/dT for pure water are calculated from the correlation of Harvey and Lemmon.[46] Properties of pure nitrogen, including $B(T)$, are calculated from the reference-quality equation of state of Span *et al.*[47]

2. Theory

For comparison with the experimental data, and to generate surrogate experimental data at different temperatures, we calculate B_{12} and ϕ_{12} from the SIMPER potential. B_{12} is calculated semiclassically including translational and rotational quantum effects to first order, as described in Ref. 48.

Having calculated the second virial coefficient as a function of the temperature, we fit it to the analytic form

$$B_{12}(T) = \sum_{i=1}^{3} c_i (T^{\star})^{d_i}, \tag{27}$$

where $T^{*}=T/(100\ \mathrm{K})$, B_{12} and the c_i have units of $cm^3\ mol^{-1}$, and the values of c_i and d_i are given in Table VI. Equation (27) fits our calculated values of B_{12} within

TABLE V. Values of $\phi_{12}=B_{12}-T(dB_{12}/dT)$ for $H_2O\cdots N_2$ derived from vapor-phase enthalpy-of-mixing data. Temperatures are given in K, and ϕ_{12} and their uncertainties $\Delta\phi_{12}$ in $cm^3\ mol^{-1}$.

T	ϕ_{12}	$\Delta\phi_{12}$	Reference	T	ϕ_{12}	$\Delta\phi_{12}$	Reference
373.12	−80	12	42	573.11	−44	21	43
380.12	−96	12	42	598.11	−20	21	43
390.12	−88	15	42	648.11	−20	15	43
400.12	−87	14	42	696.5	−20	17	45
410.12	−65	20	42	698.10	−33	17	43
423.11	−59	24	42	805.3	9	13	45
498.11	3	31	43	910.9	5	11	45
548.11	−8	41	43				

TABLE VI. Parameters for the analytic approximation, Eq. (27), of $B_{12}(T)$ for the $H_2O\cdots N_2$ complex. The c_i are in $cm^3\,mol^{-1}$ and the d_i are dimensionless.

i	c_i	d_i
1	67.595	−0.24
2	−249.83	−1.06
3	−204.38	−3.22

0.05 $cm^3\,mol^{-1}$ between 200 and 1500 K, and within 1 $cm^3\,mol^{-1}$ at higher temperatures up to 3000 K.

3. Comparison with experimental data

In Figs. 8 and 9, the calculated data are plotted alongside the experimental data, which are only available for the temperatures shown. The uncertainties in the theoretically predicted B_{12} are based on calculations using SIMPER potentials with binding energies ($E<0$) increased and decreased by 5% as in earlier works.[48] Potential energies above zero are not changed in estimating the uncertainties. This scaling of the intermolecular potential well is based on a reasonably pessimistic estimate of its uncertainty, as the difference in well depths between SIMPER and CCSD(T), and the effect of changing the basis set, are much less than 5%. The two lowest-temperature points from Kosyakov *et al.*[25] lie below the boundaries of the graph and are not shown in the figure; data from this source have also proved to be outliers in previous systems studied.[34,48] While there is some inconsistency among the experimental data sets, our calculations are consistent with the majority of sources[26,27,29–32,40] within their uncertainties. Our uncertainties are comparable to those of the most precise experiments (which only cover a narrow temperature range), and our results are significantly less uncertain than any experimental data below 273 K or above 373 K. It can also be noted that our results cover temperatures from 100 to 3000 K, providing values of B_{12} at many conditions where no experimental data exist.

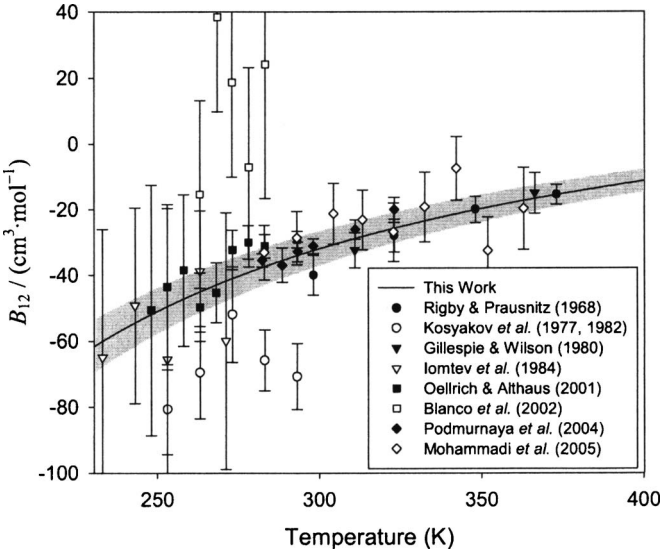

FIG. 8. Experimental and theoretically predicted (solid line) second virial coefficients at low temperatures. Shading represents the uncertainty (standard uncertainty with coverage factor of 2) of the theoretical calculation.

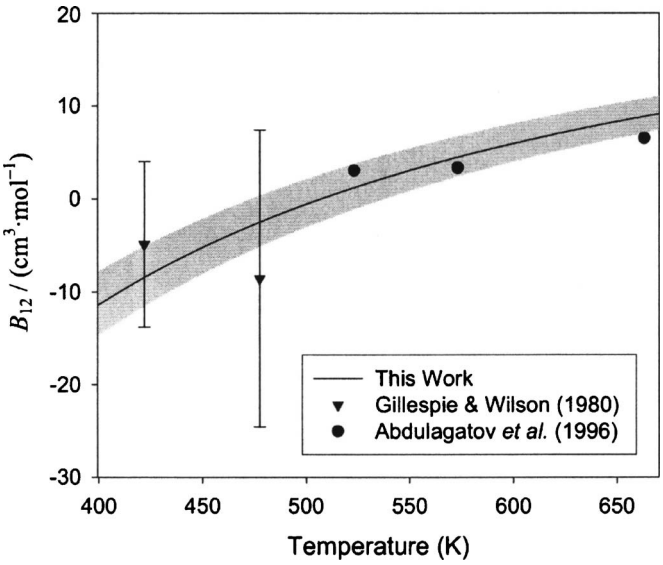

FIG. 9. Experimental and theoretically predicted (solid line) second virial coefficients at high temperatures. Shading represents the uncertainty (standard uncertainty with coverage factor of 2) of the theoretical calculation.

Figure 10 shows a similar comparison for the quantity ϕ_{12}. For this quantity, our results are again generally consistent with the experimental data, but our uncertainties are significantly smaller.

IV. DISCUSSION

The uncertainty in $B_{12}(T)$ from this work is dominated by the uncertainty in the pair potential. This estimated uncertainty (standard uncertainty with coverage factor of 2) is shown over part of its range in Figs. 8 and 9; it gradually decreases with increasing temperature throughout the range considered. Other factors affecting the calculation of B_{12}, such as higher-order quantum effects[48] and convergence of the numerical integration for B_{12}, are negligible in compari-

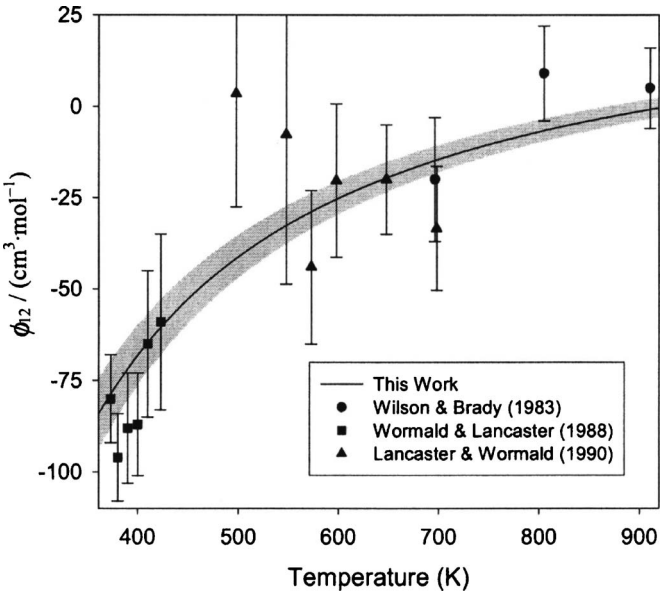

FIG. 10. Experimental and theoretically predicted (solid line) ϕ_{12}. Shading represents the uncertainty (standard uncertainty with coverage factor of 2) of the theoretical calculation.

son at the temperatures considered here. The dependence of B_{12} on the chosen fitting function is also negligible: to check this, we performed an additional fit with 198 parameters,[22] by constraining the maximum l values used in the angular expansion functions to be one less than in the original 564-parameter fit. This fit gave a weighted rms error of $\Omega = 2.2\ \mathrm{cm}^{-1}$. The difference in B_{12} calculated using the two fits was 0.5 $\mathrm{cm}^3\ \mathrm{mol}^{-1}$ at $T=100$ K, 0.3 $\mathrm{cm}^3\ \mathrm{mol}^{-1}$ at $T=300$ K, and 0.1 $\mathrm{cm}^3\ \mathrm{mol}^{-1}$ at $T=1000$ K.

Further reduction in the uncertainty of B_{12} requires refinement of the pair potential. With better computational capabilities in the future, it is likely that this uncertainty could be reduced significantly by using the SIMPER methodology with higher-level *ab initio* methods for the "low" and/or the "high" levels of calculation, and also perhaps with larger basis sets.

An additional source of uncertainty may become important at very high temperatures. Our pair calculations utilized rigid monomer structures corresponding to the vibrational ground state. At high temperatures, excited vibrational states are significantly populated. For the H_2O-N_2 pair, the lowest-lying vibration is the H_2O bend with characteristic temperature of 2290 K. The fraction of excited H_2O molecules is about 10% at 1000 K, and over 30% at 3000 K. In principle, one could include vibrational degrees of freedom in the potential energy surface and incorporate excited-state contributions into $B_{12}(T)$ with their appropriate Boltzmann weights. This would greatly increase the complexity of the calculation, but may be considered for future work. For now, we note that the change in the monomer structure is small, as evidenced by the measured[49] 1.7% decrease in the dipole moment of H_2O between the ground state and the first excited vibrational state. This suggests that we are justified in ignoring this effect at our current uncertainty levels, at least in the range of practical interest below 2000 K.

V. CONCLUSIONS

The intermolecular potential energy surface for the H_2O-N_2 interaction has been calculated at the supermolecule MP2 level of theory and then improved using the SIMPER methodology. Comparison of the surfaces at three levels of theory in low-energy regions shows that the SIMPER method is in excellent agreement with CCSD(T) calculations, while MP2 overestimates the magnitude of the interaction energies. With SIMPER, this high-accuracy surface was generated at much less computational expense than would have been required for a full CCSD(T) calculation of the surface. We note that the computational cost of SIMPER scales with system size in the same manner as the MP2 supermolecule method for each point on the potential energy surface; SIMPER also requires CCSD properties for the monomers, but this calculation only needs to be done once per monomer, not once per point, so it does not significantly affect the total computational effort.

The SIMPER potential has been used to calculate the second virial coefficient, $B_{12}(T)$, from 100 to 3000 K. The accuracy of our second virial coefficients at least equals that of B_{12} obtained from the best experiments, and our work covers a larger temperature range. It is anticipated that this work will find application in calculating thermodynamic properties of humid gases in a variety of applications, for example, in the areas of humidity standards and combustion gases.

ACKNOWLEDGMENT

This work is a partial contribution of the National Institute of Standards and Technology, not subject to copyright in the United States.

[1] H. O. Leung, M. D. Marshall, R. D. Suenram, and F. J. Lovas, J. Chem. Phys. **90**, 700 (1989).
[2] P. Sadlej, B. Rowland, J. P. Devlin, and V. Buch, J. Chem. Phys. **102**, 4804 (1995).
[3] P. Sandler, J. O. Jung, M. M. Szczęśniak, and V. Buch, J. Chem. Phys. **101**, 1378 (1994).
[4] E. M. Mas and K. Szalewicz, J. Chem. Phys. **104**, 7606 (1996).
[5] K. P. Huber and G. Herzberg, *Constants of Diatomic Molecules*, Molecular Spectra and Molecular Structure Vol. IV (Van Nostrand Reinhold, New York, 1979).
[6] T. H. Dunning, J. Chem. Phys. **90**, 1007 (1989).
[7] D. E. Woon and T. H. Dunning, J. Chem. Phys. **98**, 1358 (1993).
[8] E. N. Bichoutskaia, M. P. Hodges, and R. J. Wheatley, J. Comput. Methods Sci. Eng. **2**, 391 (2002).
[9] S. F. Boys and F. Bernardi, Mol. Phys. **19**, 553 (1970).
[10] W. H. Press, S. A. Teukolsky, W. T. Vetterling, and B. P. Flannery, *Numerical Recipes in FORTRAN: The Art of Scientific Computing* (Cambridge University Press, Cambridge, 1992).
[11] H.-J. Werner, P. J. Knowles, R. Lindh *et al.*, MOLPRO, version 2002.6, a package of *ab initio* programs, 2003; see http://www.molpro.net
[12] Certain commercial products are identified in this paper, but only in order to adequately specify the procedure. Such identification neither constitutes nor implies recommendation or endorsement by either the U.S. government or the National Institute of Standards and Technology.
[13] R. Moszynski, S. M. Cybulski, and G. Chalasiński, J. Chem. Phys. **100**, 4998 (1994).
[14] E. N. Bichoutskaia, A. S. Tulegenov, and R. J. Wheatley, Mol. Phys. **102**, 567 (2004).
[15] G. Chalasiński and M. M. Szczęśniak, Mol. Phys. **63**, 205 (1988).
[16] T. Helgaker, P. Jorgensen, and N. C. Handy, Theor. Chim. Acta **76**, 227 (1989).
[17] W. H. Adams, J. Math. Chem. **10**, 1 (1992).
[18] R. McWeeny and B. T. Sutcliffe, *Methods of Molecular Quantum Mechanics* (Academic, London, 1969).
[19] A. S. Tulegenov, Ph.D. dissertation, University of Nottingham, 2006.
[20] A. J. Stone and R. J. A. Tough, Chem. Phys. Lett. **110**, 123 (1984).
[21] R. Schinke and W. A. Lester, J. Chem. Phys. **70**, 4893 (1979).
[22] See EPAPS Document No. E-JCPSA6-126-015707 for the source code and compilation instructions for the FORTRAN subroutine described in the journal article. This document can be reached via a direct link in the online article's HTML reference section or via the EPAPS homepage (http://www.aip.org/pubservs/epaps.html).
[23] K. L. Bak, P. Jørgensen, J. Olsen, T. Helgaker, and W. Klopper, J. Chem. Phys. **112**, 9229 (2000).
[24] N. E. Kosyakov, B. I. Ivchenko, and P. P. Krishtopa, Vopr. Khim. i Khim. Tekhnol. **68**, 33 (1982).
[25] N. E. Kosyakov, B. I. Ivchenko, and P. P. Krishtopa, J. Appl. Chem. USSR **50**, 2436 (1977).
[26] M. B. Iomtev, V. G. Piskunov, and V. L. Kadzhayev, *Tables of the National Standard Reference Data Service of the USSR R88-84* (All-Union Research Institute of Technical Information, Archival Deposit No. 220, Moscow, 1984), cited in V. A. Rabinovich and V. G. Beketov, *Moist Gases: Thermodynamic Properties* (Begell House, New York, 1995).
[27] L. R. Oellrich and K. Althaus, *GERG Technical Monograph 14, Fortschr.-Ber. VDI, Series 3, No. 679* (VDI Verlag, Düsseldorf, 2001).
[28] S. T. Blanco, I. Velasco, and S. Otín, Phys. Chem. Liq. **40**, 167 (2002).
[29] M. Rigby and J. M. Prausnitz, J. Phys. Chem. **72**, 330 (1968).
[30] P. C. Gillespie and G. M. Wilson, Technical Report No. RR-41 (Gas Processors Association, Tulsa, OK, 1980).
[31] O. A. Podmurnaya, O. Gudkov, and N. Dubovikov, Russ. J. Phys. Chem.

78, 300 (2004).
[32] A. H. Mohammadi, A. Chapoy, B. Tohidi, and D. Richon, J. Chem. Eng. Data **50**, 541 (2005).
[33] M. P. Hodges, R. J. Wheatley, and A. H. Harvey, J. Chem. Phys. **116**, 1397 (2002).
[34] M. P. Hodges, R. J. Wheatley, and A. H. Harvey, J. Chem. Phys. **117**, 7169 (2002).
[35] T. R. Rettich, R. Battino, and E. Wilhelm, J. Solution Chem. **13**, 335 (1984).
[36] R. Fernández-Prini, J. L. Alvarez, and A. H. Harvey, J. Phys. Chem. Ref. Data **32**, 903 (2003).
[37] S. T. Blanco, I. Velasco, E. Rauzny, and S. Otín, Fluid Phase Equilib. **161**, 107 (1999).
[38] A. H. Harvey, A. P. Peskin, and S. A. Klein, NIST/ASME Steam Properties, NIST Standard Reference Database 10, Version 2.2, National Institute of Standards and Technology, Gaithersburg, MD, 2000.
[39] A. V. Plyasunov and E. L. Shock, J. Chem. Eng. Data **48**, 808 (2003).
[40] I. M. Abdulagatov, A. R. Bazaev, R. K. Gasanov, and A. E. Ramazanova, J. Chem. Thermodyn. **28**, 1037 (1996).
[41] P. Richards, C. J. Wormald, and T. K. Yerlett, J. Chem. Thermodyn. **13**, 623 (1981).
[42] C. J. Wormald and N. M. Lancaster, J. Chem. Soc., Faraday Trans. 1 **84**, 3141 (1988).
[43] N. M. Lancaster and C. J. Wormald, J. Chem. Eng. Data **35**, 11 (1990).
[44] C. J. Wormald and C. N. Colling, J. Chem. Thermodyn. **15**, 725 (1983).
[45] G. M. Wilson and C. J. Brady, Technical Report No. RR-73 (Gas Processors Association, Tulsa, OK, 1983).
[46] A. H. Harvey and E. W. Lemmon, J. Phys. Chem. Ref. Data **33**, 369 (2004).
[47] R. Span, E. W. Lemmon, R. T. Jacobsen, W. Wagner, and A. Yokozeki, J. Phys. Chem. Ref. Data **29**, 1361 (2000).
[48] M. P. Hodges, R. J. Wheatley, G. K. Schenter, and A. H. Harvey, J. Chem. Phys. **120**, 710 (2004).
[49] S. J. Shostak, W. L. Ebenstein, and J. S. Muenter, J. Chem. Phys. **94**, 5875 (1991).